# Magnesium Hydride Slurry: A Potential Net-Zero Carbon Dioxide Emitting Aviation Fuel

*Yi Jie Wu, Jake Scarponi, Adam Powell, Jagannath Jayachandran**

*Worcester Polytechnic Institute*

**Corresponding author*

## Abstract

A potential sustainable aviation fuel that could also absorb airborne carbon dioxide is magnesium hydride ($MgH_2$), which combusts to release magnesium oxide (MgO) and water. The MgO can react with $CO_2$ and water in the engine plume or atmosphere to form magnesium carbonate ($MgCO_3$), or magnesium bicarbonate ($Mg(HCO_3)_2$). This work describes initial results of a study to determine the potential of a slurry consisting of $MgH_2$ and an appropriate surrogate hydrocarbon jet fuel. Thermodynamic calculations were performed to compare the thermal combustion performance of $MgH_2$ slurries with *n*-dodecane (*n*-$C_{12}H_{26}$) at varying ratios using conditions at aircraft cruising altitude. The heat of combustion as well as the mass and volume of each fuel required to reach target equilibrium temperatures at a given fuel equivalence ratio and oxidizer (air) mass are compared. $MgH_2$ combustion's lower heating value (LHV) is 33.8% lower than *n*-$C_{12}H_{26}$ per unit mass, but 22% higher per unit volume. Thermodynamic models show that, relative to LHV, $MgH_2$/*n*-$C_{12}H_{26}$ slurry requires 2-5% less fuel to reach a typical engine combustion temperature than *n*-$C_{12}H_{26}$ under these engine operating conditions, and up to 25% less fuel at higher engine combustion temperatures. Based in part on this result, the Breguet range equation shows that a hydrocarbon-$MgH_2$ slurry fuel should achieve up to 8% longer aircraft range than the same volume of the hydrocarbon fuel, though other aircraft changes required to accommodate the denser fuel could offset that range extension. This is also over 2.5 times the range of liquid ammonia, and 3.5 times the range of liquid hydrogen, if those fuels could be used in the same tanks. Feasibility of the $CO_2$ absorption process and sustainable $MgH_2$ production are also discussed.

*Keywords: Sustainable aviation, aviation fuel, aerospace, metal combustion, magnesium hydride, jet fuel, slurry fuel, carbon capture, net-zero emissions*

## 1. Introduction

Carbon dioxide emissions from the aviation sector amount to about 2.5% of the world's fossil fuel emissions. With approximately 5% annual growth, these particular emissions are estimated to triple by 2050 [1, 2]. Biofuels exhibit net-zero greenhouse gas (GHG) emissions in principle, but in practice require GHG-intensive fertilizers and compete for land use and fresh water with food production and carbon-sinking forests [3]. Some other alternatives to traditional hydrocarbon fuels, such as batteries, liquid hydrogen, and liquid ammonia do not have the energy/volume (E/V) or/and energy/mass (E/M) (see Fig. 1) to support intercontinental commercial travel in configurations similar to today's aircraft, making the aviation industry a particularly difficult sector to decarbonize.

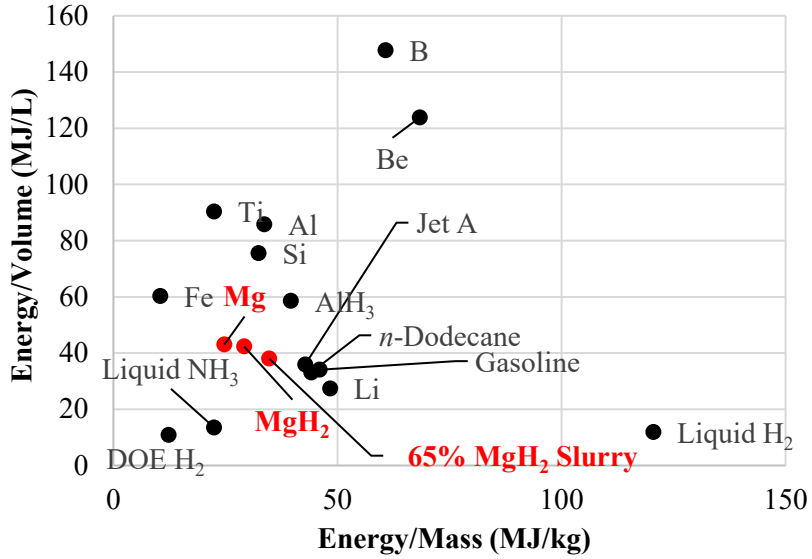


Figure 1: Comparison of E/V and E/M of slurry, other fuels and other metals. [4]

Metals can store energy at higher E/V and comparable E/M to hydrocarbons [4], as shown in Fig. 1. In addition, many metals have much higher adiabatic flame temperatures than hydrocarbons [4, 5], potentially leading to higher specific thrusts and combustion efficiencies as new material and technological developments enable higher engine temperatures. Energy release can be achieved by reacting metals with compounds or mixtures that contain $O_2$ (e.g., $CO_2$, $H_2O$, air), creating oxides. Oxidation of certain metals not only avoids $CO_2$ emissions, but their more basic oxides can potentially absorb $CO_2$ by formation of carbonates. In particular, the hydrides of Groups I-III metals have high energy densities and basic oxides which form carbonates.

Light metals such as beryllium and metalloids such as boron with high energy content (see Fig. 1) are both expensive and known to be toxic; inhalation of nanoparticles can cause extensive nerve damage. Aluminum has a high energy density, but is linked to Alzheimer's disease [6, 7, 8], and silicon and silicon dioxide is linked to silicosis [9]. Titanium is less abundant; its reduction from ore to metal is inefficient and expensive [10]. On the other hand, magnesium is an important mineral that the human body uses for metabolic reactions and is believed to improve symptoms of migraine headaches [11]. $Mg(OH)_2$ is used for treating acid indigestion and constipation. MgO and $MgCO_3$ have Lethal Dose 50 (mass per unit body mass that resulted in the death of 50% of the group of test rats) values of 4 g/kg and 8 g/kg, making them practically non-toxic. Kuschner et al. [12] studied the pulmonary effects of inhalation of fine and ultrafine MgO particles, concluding that inhalation of these particles resulted in no inflammatory response from respiratory organs and no toxicity. While these studies of Mg and MgO show that they pose no significant health risks to humans, more research is required in order to conclusively deduce that inhalation of these particles is completely safe.

Slurries of micron-sized metal particles suspended in liquid hydrocarbon fuels are pumpable and relatively safe compared to metal powders, which pose strong fire hazards. However, investigations of metal slurry combustion in practical combustors have revealed low combustion efficiencies, sometimes less than 50% [13]. This has been attributed to the slow combustion of agglomerate formed from the micron-sized metal particles, after the vaporization and combustion of the liquid hydrocarbon from the droplets [13]. The consumption of the metal agglomerate is limited by the surface area available for vaporization/reaction. Using a metal hydride instead can accelerate the combustion process as the hydride, under high heating rates relevant to combustion, dissociates before burning, releasing gaseous hydrogen, leading to increased metal particle porosity, fragmentation, or explosion, and thus increasing surface area. Experimental studies [14, 15, 16] revealed that micron sized *a*-$AlH_3$ particles ignited at substantially lower temperatures compared to similar sized Al particles. Furthermore, they observed jetting, particle fragmentation and explosion, leading to faster combustion.

The adiabatic flame temperature of Al is ~4000 K, while that of Mg is ~3400 K. Unlike aluminum, use of Mg also has potential for net-zero to net-negative emissions due to the ability of its combustion product MgO to react with atmospheric $CO_2$, resulting (in a way) in atmospheric $CO_2$ capture ($Al_2O_3$ does not form stable compounds with $CO_2$). Its hydride counterpart, $MgH_2$ can also combust in an oxidizer environment, potentially at higher rates and efficiencies. Vigeholm et al., also have studied the capabilities of Mg to absorb hydrogen at various temperatures and pressures [17]. $MgH_2$ also has 15% higher E/M (see Table 2) than pure Mg, while having almost the same E/V. Brown et al. synthesized $MgH_2$-hydrocarbon slurries cost-effectively [18], and a slurry of $MgH_2$ in mineral oil has already been demonstrated to have capabilities as a rechargeable energy storage technology [19].

Based on the above, we propose a safe and pumpable slurry fuel using a hydrocarbon fuel, optionally from bio-derived sources, with $MgH_2$ particles, whose MgO combustion product absorbs $CO_2$ in the atmosphere. To this end, we: (1) perform thermodynamic calculations to determine the maximum heat release and how it compares to a hydrocarbon fuel; (2) develop a combustor model to evaluate changes in engine performance due to the formation of solid MgO particles; and (3) perform calculations to estimate the dynamics of MgO particles in the atmosphere and how reactions with $CO_2$ will occur. Finally, we conclude with a discussion of challenges, both scientific and engineering, that must be addressed. Calculations show a Mg:C ratio of 1:1 would suffice for net zero emissions within the scope of the flight, assuming all the MgO emitted will react with $CO_2$ before it settles out of the atmosphere.

## 2. Methods (computational approach)

E/M and E/V calculations are performed assuming complete combustion of the fuel under constant temperature, $T = 298$ K, and pressure, $P = 1$ bar, conditions. *n*-Dodecane ($n$-$C_{12}H_{26}$) is chosen as a surrogate for jet fuel for all thermodynamic analyses [20, 21]. The calculations performed are for the lower heating values (LHV), assuming that the water produced is in gaseous state. Since MgO (and not $MgCO_3$) is the stable combustion product for $T > 620$ K (see Sec. 3.2 and 3.7), we use MgO as the stable product for the LHV calculations.

The following represent the stoichiometric reactions for complete combustion of *n*-$C_{12}H_{26}$, Mg, $MgH_2$, and the $MgH_2$-jet fuel slurry.

$$C_{12}H_{26}(g) + 18.5\,(O_2(g) + (79/21)\,N_2(g) \rightarrow 12CO_2(g) + 13H_2O(g) + 69.56\,N_2(g)$$

$$Mg(s) + 0.5\,(O_2(g) + (79/21)\,N_2(g) \rightarrow MgO(s) + 1.88\,N_2(g)$$

$$MgH_2(s) + 1\,(O_2(g) + (79/21)\,N_2(g) \rightarrow MgO(s) + H_2O\,(g) + 3.76\,N_2(g)$$

$$x\,MgH_2 + y\,n\text{-}C_{12}H_{26}\,(g) + (x + 18.5y)\,(O_2 + 3.76N_2) \rightarrow x\,MgO\,(s) + 12y\,CO_2\,(g) + (x + 13y)\,H_2O(g)$$

Where x and y detonate the moles of $MgH_2$ and *n*-$C_{12}H_{26}$ respectively. The post combustion state in gas-turbine combustors will however be different given the variety of species present due to considerations based on the second law of thermodynamics, for example the effects of product dissociation at high temperatures [22]. Therefore, detailed thermodynamic calculations, including all possible species, are also performed to accurately estimate the thermodynamic state at the exit of a typical gas-turbine combustor, utilizing constant *P* and adiabatic constraints. The functionalities implemented in Cantera, an open-source thermo-chemistry toolkit, were utilized for these computations [23]. The species considered and Python scripts used to perform calculations are included in the Supplementary Material. The following is a list of the major or most relevant species:

Hydrocarbon-relevant species: *n*-$C_{12}H_{26}$, $O_2$, CO, $H_2$, $CO_2$, $H_2O$ (all gas phase)

Mg-relevant species: Mg (solid, liquid, and gas phase), MgO (s), $MgCO_3$(s), $Mg(OH)_2$(s)

Thermodynamic data for the different species were obtained from the NIST Chemistry WebBook [24], the database of Burcat [25], and the compilation by Wang et al. [26]. Fuel is typically injected into the combustor in liquid state. In order to simplify the calculations, we utilize the thermodynamic properties of gaseous *n*-$C_{12}H_{26}$. This is justified as the enthalpy of vaporization is negligible (~0.6%) compared to the heat of combustion [27].

Parametric analysis was performed for a range of equivalence ratios, $0.1 < \phi < 1.0$, which covers fuel-lean operation that is relevant to gas-turbine operation. $\phi$ = 1.0 represents combustion at the stoichiometric fuel-to-oxidizer ratio. The value of □ is determined by Eqn 1 where $M_{Fuel}$ is the mass of the fuel and $M_{Oxdizier}$ is the mass of the oxidizer. When performing calculations for □ the reaction between the metal hydride in the slurries and its oxidizer are also accounted for. As most of the fuel is consumed at design cruise conditions, the thermodynamic conditions at the combustor inlet (compressor outlet) are estimated to be $P$ = 1953 kPa and $T$ = 761 K. These values are calculated assuming steady flight at ~10.7 km, where conditions are approximately 225 K and 25 kPa. A flight Mach number of 0.8 and overall pressure ratio of 50 were assumed, which are typical in modern passenger aircraft like the Boeing 787 [28].

1. $$\phi = \frac{\left(\frac{M_{Fuel}}{M_{Oxidizer}}\right)_{Actual}}{\left(\frac{M_{Fuel}}{M_{Oxidizer}}\right)_{Stoich}}$$

Calculations are performed for three different fuels: 1) $n$-$C_{12}H_{26}$, a surrogate for typical jet fuel; 2) slurry with 65% $MgH_2$ and 35% $n$-$C_{12}H_{26}$ by mass, equivalent to 1:1 Mg:C ratio, which is required to achieve "net-zero" carbon emissions, where the amount of $CO_2$ that reacts with MgO in the atmosphere equals that produced during the combustion of the hydrocarbon fraction in the slurry; and 3) slurry with 55% $MgH_2$ and 45% $n$-$C_{12}H_{26}$ by mass, which will help understand the effect of amount of $MgH_2$ loading on the equilibrium combustion characteristics of the slurry.

Since MgO is a major product of slurry combustion and is a solid, a larger pressure drop could result across the combustor relative to the traditional jet fuel due to the relatively lower moles of gaseous combustion products. Specific thrust is a function of flow velocities (Eqn 2), which are expected to decrease with a greater loss in pressure.

2. $$F = \dot{m}_e V_e - \dot{m}_0 V_0 + (p_e - p_0)A_e$$

In Eqn 2, $F$ is the thrust, $V_e$ is the exit velocity of the stream, $V_0$ is the free stream velocity, $\dot{m}_e$ is the mass flow rate of the exit stream, $\dot{m}_0$ is the mass flow rate of the free steam mass flowrate, $A_e$ is the area of the engine, $p_e$ and $p_0$ are the combustor exit and inlet pressures respectively.

In order to evaluate the pressure drop, a constant area combustor model was developed, similar to a Rayleigh flow model and it assumes the engine is a turbojet [29]. Conservation equations of mass, momentum, and energy were solved simultaneously across a one-dimensional control volume. The inlet conditions corresponded to a mixture of fuel and air at a specified thermodynamic condition at the engine compressor exit. Chemical equilibrium was enforced at the exit of the control volume using Cantera [23]. Newton's method was used to solve the set of nonlinear equations. Furthermore, cycle analysis was performed to determine the effect of the pressure drop on the specific thrust for a turbojet engine. These calculations are performed numerically using a python script which can be found in the supplementary materials. Thermodynamic property variation with temperature and changes in composition were taken into account using Cantera [23], and the devices were assumed to operate in an ideal manner.

## 3. Results and Discussion

### *3.1. Energy/Mass and Energy/Volume*

Values of E/M and E/V for A1 jet fuel, *n*-$C_{12}H_{26}$, Mg, $MgH_2$, 55% $MgH_2$ slurry, and 65% $MgH_2$ slurry are calculated and listed in Table 2. As expected, A1 jet fuel and *n*-$C_{12}H_{26}$ have similar E/M and E/V values [20, 21]. $MgH_2$ has 32% lower E/M than *n*-$C_{12}H_{26}$ but 22% higher E/V. It is important to note that $MgH_2$ has an E/M that is 18% higher compared to Mg, signifying another advantage of using $MgH_2$ in the slurry. The 55% $MgH_2$ slurry compares more favorably with *n*-$C_{12}H_{26}$ in terms of E/M as expected since it contains 35% *n*-$C_{12}H_{26}$ but the advantage in E/V is lowered to 10%.

| Fuel | E/M (MJ/kg) | Δ, % Relative to *n*-Dodecane | E/V (MJ/liter) | Δ, % Relative to *n*-Dodecane |
|---|---|---|---|---|
| A1 jet fuel | 43.15 | — | 34.6 | — |
| *n*-Dodecane (l) | 44.1 | — | 33.1 | — |
| Mg | 24.8 | -43% | 43.0 | +24% |
| $MgH_2$ | 29.2 | -33.8% | 42.3 | +22% |
| 55% $MgH_2$ Slurry | 35.9 | -18.6% | 36.7 | +10.9% |

Table 1: Specific LHV enthalpies (E/M) and enthalpy densities (E/V) of A1 jet fuel, n-$C_{12}H_{26}$, Mg, $MgH_2$, and $MgH_2$-dodecane slurries.

| | | | | |
|---|---|---|---|---|
| 65% $MgH_2$ Slurry | 34.4 | -22.0% | 38.0 | +14.8% |

172

173 ***3.2. Post combustion state***

174 Chemical Equilibrium calculations, under constraints of constant $P$ and enthalpy, are performed to
175 estimate the exit conditions of gas turbine combustor for the different fuels. Combustion inlet conditions of
176 $P = 20$ bar and $T = 761$ K are utilized (see Sec. 2).

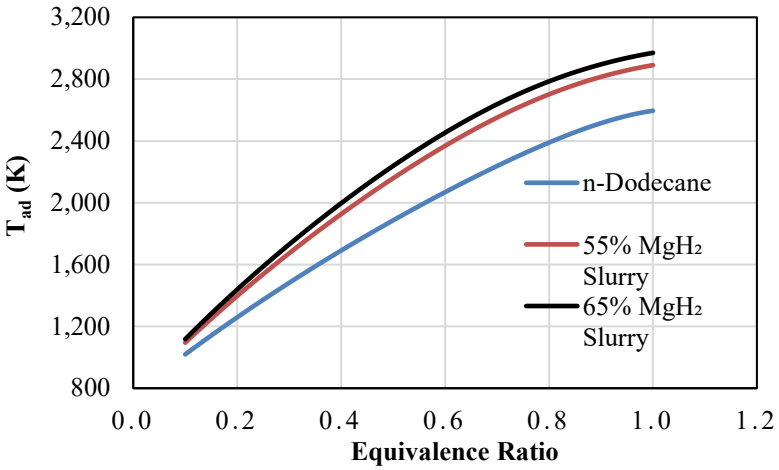


Figure 2: $T_{ad}$ as a function of $\phi$ at a $T_{inlet}$ of 761 K and a $P_{inlet}$ of 20 bar.

Fig. 2. demonstrates the variation of combustor exit temperature ($T_{ad}$) as a function of $\phi$ for the the 65% $MgH_2$ slurry, the 55% $MgH_2$ slurry, and *n*-$C_{12}H_{26}$. *n*-$C_{12}H_{26}$ has the lowest $T_{ad}$, followed by the 55% $MgH_2$ slurry and the 65% $MgH_2$ slurry, across all $\phi$. The highest possible temperature is reached at $\phi \sim 1.0$, when just the right amount of $O_2$ is present to completely oxidize the fuel. It is important to note that the slurries can be used to achieve $T_{ad}$ in excess of 2620

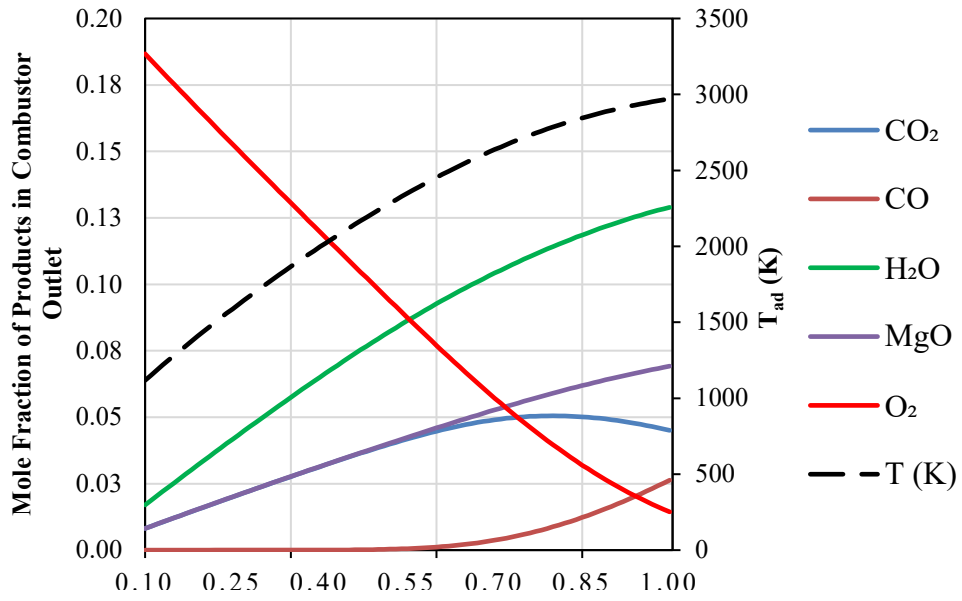


Figure 3: Mole fraction of various major species as a function of equivalence ratio $\phi$ at a $T_{inlet}$ of 761 K and a $P_{inlet}$ of 20 bar using the 65% $MgH_2$ slurry. $T_{ad}$ is also shown.

K (limit for $n$-$C_{12}H_{26}$) of up to ~3000 K for the specified initial conditions. A decrease in sensitivity of $T_{ad}$ to $\phi$ is observed as $\phi$ approaches 1.0 ($T_{ad}$ decreases more gradually). This is due to dissociation of the combustion products, specifically $CO_2$ (g), $H_2O$ (g), and to a very small extent MgO (s). Typical gas turbine combustors operate at $\phi$ values between 0.2 to 0.5 so that turbine inlet $T$s are below 2000 K, a limitation imposed by the current level of turbine blade technology.

Fig. 3. depicts the mole fraction of major species at the post combustion state for 65% $MgH_2$ slurry as a function of the equivalence ratio. $H_2O$ is the most prevalent species in this case since the combustion of both the hydrocarbon and $MgH_2$ produces it. More significantly, the ratio of MgO to total carbon is 1:1 as expected since 65% $MgH_2$ is carbon neutral should MgO react with $CO_2$ at the exhaust. At a range of $\phi$ between 0.5 and 0.6, the mole fraction of $CO_2$ decreases and CO increases. This is a sign of dissociation of the former, in line with the observation that at significantly higher $T_{ad}$, hydrocarbon fuels lose some efficiency due to incomplete combustion of CO.

### *3.3. Fuel consumption: Mass*

A better way to compare the thermodynamic performance of the slurry to $n$-$C_{12}H_{26}$ is to determine the amount of each fuel that must be added to a fixed flow rate of air to result in a particular post-combustion $T_{ad}$. Fig. 4 depicts the ratio of slurry mass to $n$-$C_{12}H_{26}$ mass to achieve a specified $T_{ad}$. The y axis is determined by the mass of slurry required to reach a $T_{ad}$ relative to the mass required for $n$-dodecane to reach that $T_{ad}$. Note that the initial $T$ and $P$ values used for the calculations are the same as those used to generate Fig. 2. It is evident that ~24% more mass of the slurry is required to attain the same $T_{ad}$. This result is consistent with the trends

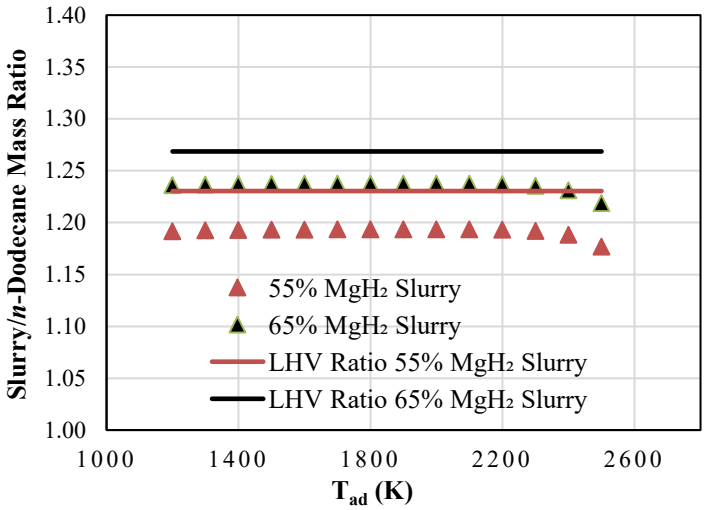


Figure 4: Ratio of slurry mass to n-$C_{12}H_{26}$ mass to achieve a target $T_{ad}$ assuming a $T_{inlet}$ of 761 K and $P_{inlet}$ of 20 bar. The ratio of their LHV values (per unit mass, see Sec. 3.1) assuming standard conditions are also included.

obtained from the E/M calculations performed (see Table 1) assuming complete combustion. The ratio starts to drop at higher $T_{ad}$, most likely due to incomplete combustion resulting from dissociation of $CO_2$ (g), and $H_2O$ (g).

Also plotted in Fig. 4 are the ratios of the lower heating values (LHV) of the slurries to *n*-$C_{12}H_{26}$. Even though the trends are similar between the ratios calculated using detailed equilibrium calculations and ratios of LHVs, there is ~5% difference between the two. This is primarily due to neglecting changes in specific heat capacity with temperature and dissociation of, in decreasing order, $CO_2$ (g), $H_2O$ (g), and MgO (s) for LHV calculations. The dissociation effects become more important at higher $T_{ad}$s, illustrated by the decreasing values of ratios at $T_{ad} > 2200$ K.

### *3.4. Fuel consumption: Volume*

One advantage of the slurry is its higher density and thus E/V. The density of pure $MgH_2$ is 1450 kg/m$^3$, nearly double that of liquid *n*-$C_{12}H_{26}$ which is 750 kg/m$^3$. The 65% $MgH_2$ slurry has a density of 1093 kg/m$^3$, which is ~45% higher than *n*-$C_{12}H_{26}$. In order to better understand the effect of higher fuel density on performance, Fig. 5 plots the ratio of volume between two compositions of slurries to the volume of *n*-$C_{12}H_{26}$ required to achieve a particular $T_{ad}$ (for a fixed flow rate of air). It is evident that a smaller volume of slurry can be burned compared to *n*-$C_{12}H_{26}$ to reach a target $T_{ad}$. For a fixed fuel tank size, the slurry provides an aircraft with more total energy content, which can increase aircraft range (discussed in section 3.6). Over a range of $T_{ad}$s between 1200~2500 K, the slurries require 13 to 17% less volume compared to *n*-$C_{12}H_{26}$.

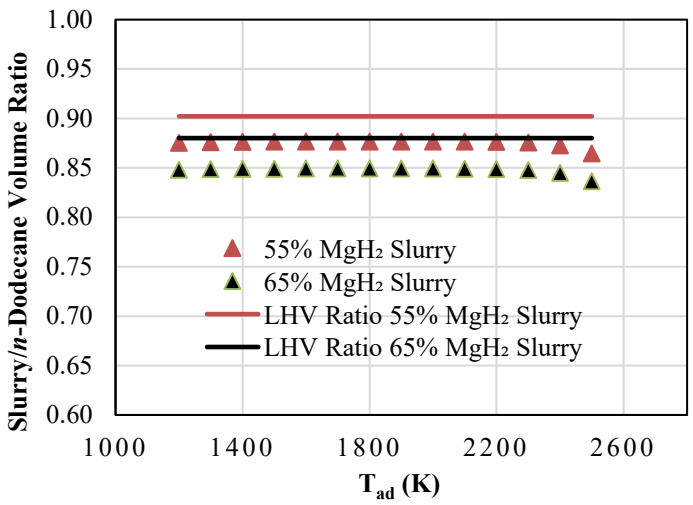


Figure 5: Volume ratio comparison of n-$C_{12}H_{26}$/slurry at a range of target $T_{ad}$, including the ratio of their LHV E/V values calculated at standard conditions.

### *3.5. Pressure Drop and Thrust*

The impact of the formation of solids on the engine performance is evaluated by estimating the $P$ drop across the combustor when the different fuels are used. Figure 6 plots the fractional $P$ loss experienced across the combustor over a range of turbine inlet (i.e., combustor exit) $T$s for the 65% $MgH_2$ slurry and $n$-$C_{12}H_{26}$, respectively. The analysis assumes thermodynamic conditions similar to those mentioned in Section 2, and a Mach number of 0.1 at the inlet of the combustor. Over a range of $T_{ad}$ between 1600-2500 K ($0.35 < \phi < 0.90$), the difference in pressure drop when the 65% $MgH_2$ slurry is used instead of $n$-$C_{12}H_{26}$ to attain the same $T_{ad}$, is negligible, despite the formation of solids in the case of the slurry. This is due to the large amount of nitrogen in the fuel/air mixture (~76% by mass) that does not react. For slurry combustion, the solid particles, mainly MgO, make up only ~3-4% by mass of the combustion products, depending on $\phi$.

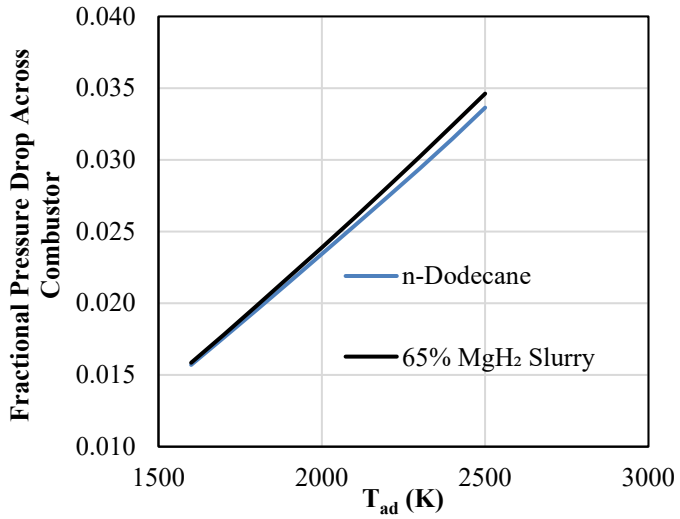


Figure 6: Fractional pressure drop across the combustor for n-$C_{12}H_{26}$ and 65% $MgH_2$ slurry for a range of target $T_{ad}$.

Cycle analysis performed to determine the impact of the pressure loss over the engine revealed a difference in thrust is less than 1% when the 65% $MgH_2$ slurry is used instead of $n$-$C_{12}H_{26}$ to attain the same post combustion temperature. Other (second order) effects like slippage between the fluid flow and particles, decrease in turbine efficiency, etc. have not been considered in this analysis and are beyond the scope of this study.

### *3.6. Range Calculations*

Range calculations are performed using the Breguet range equation (Eqn. 3), which uses the mass of the aircraft with empty and fuel-filled fuel tanks. Here $L$ and $D$ are the lift and drag coefficients respectively, and $\eta_o$ is the propulsion efficiency. These values are assumed to be constant and thus they are canceled in Eqn 3. $M_{Empty}$ is the mass of the airplane when empty and $M_{Full}$ is the mass of the aircraft with

fuel tanks filled. Assuming a typical Boeing 787 jet, the mass of the empty jet is assumed to be 380000 kg and 560000 kg when filled with fuel. From the results of Eqn. 3, the range of an aircraft fueled with the hydride slurry relative to that fueled with $n$-$C_{12}H_{26}$ can be found using Eqn. 4, where $Q_c$ is the respective fuel E/M. Also assumed is similar efficiencies and (L/D) for the different fuel cases.

3. $$Range = \frac{\eta_o LHV}{g}\left(\frac{L}{D}\right) ln\left(\frac{M_{Empty}}{M_{Full}}\right)$$

4. $$Relative\ Range = \frac{LHV_{c,Slurry}}{LHV_{c,n-Dodecane}} \frac{ln\left(\frac{Mass_{Empty}}{Mass_{Full}}\right)_{Slurry}}{ln\left(\frac{Mass_{Empty}}{Mass_{Full}}\right)_{Dodecane}}$$

This metric allows for comparison between the range capabilities of the two fuels given the fuel tank size.

The Boeing 787 with empty fuel tanks weighs around 380 tons, and when full, around 560 tons. This sets the fuel weight at 180 tons and using the standard density of $n$-$C_{12}H_{26}$ of 750 kg/m$^3$, the fuel tank volume is estimated to be 240 m$^3$. Replacing it with slurry mixtures will increase the overall net weight of the aircraft depending on mixture composition due to the increased density of the slurry. The 65% $MgH_2$ slurry has a density of 1093 kg/m$^3$ which means a 240 m$^3$ fuel tank would carry ~262.3 tons of the mixture.

However, the $MgH_2$ slurry however can provide more range given the same volume because it has a higher E/V, which can be beneficial in certain cases. The 65% $MgH_2$ slurry has a density of 1093 kg/m$^3$, around 31% more than $n$-$C_{12}H_{26}$, and E/V of 38.0 MJ/liter, about 15% more than $n$-$C_{12}H_{26}$. On the other hand, it takes 24% more 65% $MgH_2$ slurry mass to reach 1800 K than $n$-$C_{12}H_{26}$ mass (see Fig. 4). The combined effect, which is evaluated using the Breguet equation, indicates that range is about 8.0% higher for the 65% slurry compared to $n$-$C_{12}H_{26}$ – which is somewhat

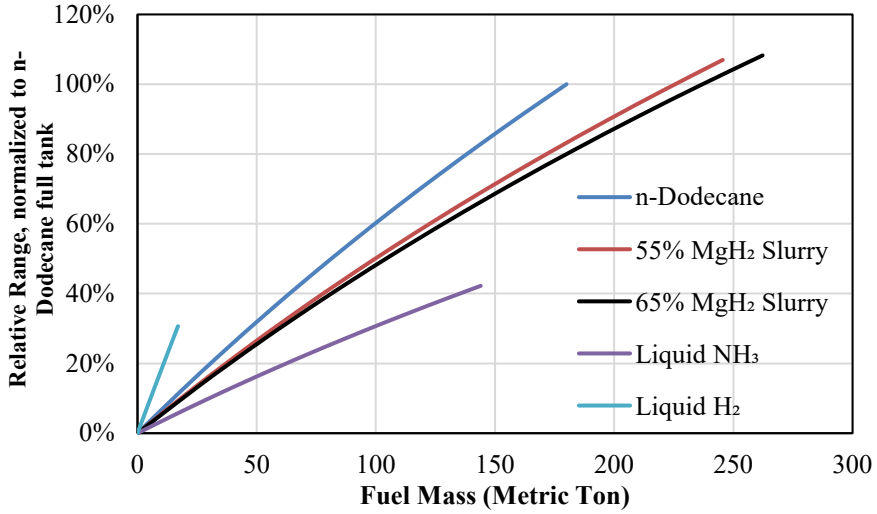


Figure 7: Relative range comparison with fuel mass assuming the aircraft to be the 787 (for a fixed fuel tank volume)

less than the 15% higher energy density, but more than the 4.5% which one would predict based on the Breguet equation and LHV energy density. Fig. 6 depicts the relative ranges of the fuels.

Also included in Fig. 7 are relative ranges for liquid ammonia ($NH_3$) and liquid $H_2$, two candidate carbon-free fuels. Liquid $H_2$ and liquid $NH_3$ ranges are ~30% and ~42% relative to *n*-$C_{12}H_{26}$.While the overall mass of the aircraft would decrease due to the high E/M of these 2 fuels, larger fuel tanks would be required for long flights which can impact the performance of the flight. In addition, if engine materials continue to advance with better physical, thermal properties at higher temperatures, the hydride could outperform conventional jet fuel, $H_2$, and $NH_3$ by even more.

### *3.7. Atmospheric Effects*

Engine exhaust should consist of mostly submicron MgO particles, water vapor, $CO_2$, and nitrogen [30]. Any unburned Mg could react with airborne nitrogen ($N_2$) rather than $O_2$ to produce magnesium nitride ($Mg_2N_3$). However, $N_2$ can be considered an inert gas, especially in the presence of $O_2$. Y. Chunmiao et al. experimented with Mg reactions in mixtures with varying concentrations of $O_2$ and $N_2$. It was conclusively found that, like all metals, magnesium tends to undergo oxidation rather than nitridation [31]. Also, neither Mg nor $Mg_2N_3$ are produced in a significant amount during combustion under fuel-lean engine operation, according to the model discussed in previous sections.

To further support this, Fig 8. compares the Gibbs free energy of possible states at a range of temperatures. The major products of stoichiometric slurry combustion at *P* of 0.1 MPa are $MgO_{(s)}$, $CO_2$, $H_2O$ and $N_2$. In the exhaust, MgO can remain inert (described by Eqn. 3), react with $CO_2$ to form $MgCO_3$ (Eqn. 4), react with $H_2O$ to form $Mg(OH)_2$ (Eqn. 5), or react with $N_2$ to form $Mg_3N_2$ (Eqn. 6). The reactions are written considering 1000 moles of air and $\phi = 1.0$.

$$6.88C_{12}H_{26(g)} + 82.7MgH_{2(s)} + 210O_{2(g)} + 790N_{2(g)} \rightarrow 82.7MgO_{(s)} + 172.2H_2O_{(l)} + 82.6CO_{2(g)} + 790N_{2(g)} \quad (3)$$

$$82.7MgO_{(s)} + 82.6CO_{2(g)} + 172.2H_2O_{(l)} + 790N_{2(g)} \rightarrow 82.6MgCO_{3(s)} + 0.1MgO_{(s)} + 172.2H_2O_{(l)} + 790N_{2(g)} \quad (4)$$

$$82.7MgO_{(s)} + 172.2H_2O_{(l)} + 790N_{2(g)} + 82.6CO_{2(g)} \rightarrow 82.7Mg(OH)_{2(s)} + 82.5H_2O_{(l)} + 790N_{2(g)} + 82.6CO_{2(g)} \quad (5)$$

$$82.7Mg_{(s)} + 790N_{2(g)} + 41.3O_{2(g)} + 172.2H_2O_{(l)} + 82.6CO_{2(g)} \rightarrow$$
$$27.6Mg_3N_{2(s)} + 762.4N_{2(g)} + 41.3O_{2(g)} + 172.2H_2O_{(l)} + 82.6CO_{2(g)} \quad (6)$$

Across the entire range of $T$, the nitride state is the least stable, supporting the conclusion that Mg is more likely to undergo oxidation rather than nitridation. For $T > 620$ K, MgO is the most stable product, whereas for $T < 620$ K, $MgCO_3$ is most stable. $MgCO_3$ could form in the engine exhaust plume and atmosphere where $T < 600$ K. The exhaust mixes with atmospheric air and cools down to ~225 K within seconds of being ejected from the nozzle. However, the reaction of MgO with $CO_2$ is expected to progress slowly due to low $T$ and low mole fractions of $CO_2$ in the upper atmosphere. Consideration of kinetics can complicate the analysis, and reactions with water vapor also needs to be taken into account.

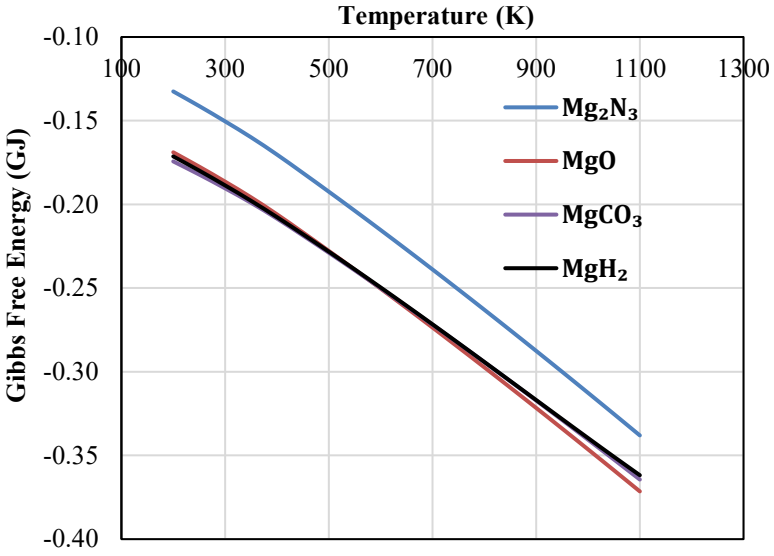

Figure 8: Comparison of Gibbs free energy of possible product compositions at T between 200 to 1100 K.

Based on this thermodynamics assessment, to understand the kinetics of this MgO reaction, we propose a cooperative $CO_2$-water adsorption, dissolution, diffusion mechanism for the MgO-$CO_2$-water reaction in the atmosphere. That is, $CO_2$ and water adsorb onto an MgO particle surface, creating a layer of hydrated $MgCO_3$ or $Mg(HCO_3)_2$ that chemically attracts further water adsorption; MgO dissolves into the resulting solution as $Mg(OH)_2$ while $H_2O$ and $CO_2$ continue to adsorb onto the solution droplet.

Possible limiting steps for this mechanism include $CO_2$ and water adsorption, MgO dissolution, and diffusion of $Mg^{2+}$, $CO_3^{2-}$ and $HCO_3^-$ ions through liquid water. As described in the supplementary materials, all of these mechanisms operate on time scales much faster than the atmospheric residence time of particles. These particles will likely be submicron, since $MgH_2$ particles in the unburned fuel are roughly

1 μm in diameter. As also described in the Supplement, atmosphere-aqueous solution thermodynamics indicate that each $Mg^{2+}$ ion in solution leads to the absorption of 1-2 $CO_2$ molecules from the atmosphere, in addition to any $CO_2$ which would be absorbed without the Mg. At high $Mg^{2+}$ concentration, this corresponds to dissolved $Mg(HCO_3)_2$, and at low $Mg^{2+}$ concentration, to dissolved $MgCO_3$. As described in the supplement, the most prevalent species depends on atmospheric residence time as it relates to particle size: if small droplets settle out of the atmosphere fast, then they will be $Mg(HCO_3)_2$; if large droplets, then $MgCO_3$. In either case, upper-troposphere injection of submicron MgO particles should bring down at least as many moles of $CO_2$ as Mg. A 65% mass mixture of $MgH_2$ and hydrocarbon fuel could thus achieve net-zero emissions in the scope of the flight, and any additional $MgH_2$ and/or application of biofuel could potentially yield net-negative emissions.

Nevertheless, further study into the kinetics of these reactions is required as the low atmospheric temperature and pressure could impact the rate at which the reaction occurs. However, some estimations show micron-sized particles could have residence times as high as 100 days in the atmosphere, which could provide ample time for the reactions to proceed. [32]

### *3.8. Magnesium Hydride Production and Life Cycle Impacts*

Understanding GHG emissions impact requires consideration of a product's life cycle. In this case, life cycle emissions of slurry fuel depend strongly on the methods of magnesium and hydrogen production. Combining them into $MgH_2$ might be as simple as atomizing Mg metal in an atmosphere which includes $H_2$. [18] Most hydrogen is produced today by steam reforming of natural gas with high GHG emissions. Future hydrogen technologies from vehicle fuel cells to HYBRIT ironmaking require "green hydrogen" produced by electrolysis using renewable or nuclear energy in order to reduce life cycle GHG emissions, and that will be the case here as well. Fortunately, green hydrogen costs are projected to fall significantly in the coming decades [33].

Achieving overall net zero emissions requires deployment of new magnesium production technology. For example, the Alliance Magnesium process [34] and magnesium oxide reduction similar to

Hall-Héroult aluminum with a reactive cathode and multiple effect distillation [35] could meet this goal, provided raw material selection and drying and calcination energy source are suitable, as described in the supplement. However, present emissions are 2.5-10 kg $CO_2$e/kg Mg for electrolytic technologies (much of this from fossil fuel heating), and 20-25 kg $CO_2$e/kg Mg for thermal reduction using ferrosilicon [34, 36, 37]. With each kg Mg in slurry fuel absorbing 1.8-3.7 kg $CO_2$ from the atmosphere – and reducing overall $CO_2$ emissions by 1.3-1.5 times this amount for fossil fuels – making this a sustainable choice rules out thermal reduction and requires low-emissions electrolysis.

Current water desalination plants around the world could produce up to 110 Mt/a magnesium from their seawater concentrate, which is about half of what would be needed to replace 2019 levels of jet fuel consumption with 65% $MgH_2$ slurry.

## 4. Future Work

This paper has presented thermodynamic models indicating that a hydrocarbon-$MgH_2$ slurry fuel will likely achieve the high flame temperature, specific thrust, efficiency, and reaction with atmospheric $CO_2$ needed to achieve dramatic reduction, elimination, or even reversal of GHG impacts of flight without compromising aircraft range. But multiple issues will complicate its use.

*Slurry stability:* Precautions will be required to ensure that particles do not settle in the slurry, for example by using dispersants such as oleic acid, and to minimize hydrogen evolution in storage. The suspension has been proven to be very stable when produced with mineral oil [18] but stability in lighter hydrocarbons, including *n*-$C_{12}H_{26}$ and jet fuel, is currently not well understood. Parametric studies also have demonstrated that metal-jet fuel slurry with metal particle loading up to 70% by mass can be prepared to have stability and flow properties acceptable for flight applications; additives (less than 1%, like metal soaps) increase stability and dispersants decrease viscosity [38].

*Slurry atomization*: It will be necessary to atomize the slurry in order to achieve mixing and effective combustion. But slurries have high viscosity and are held together by capillary effects of surface tension. An effervescent or ultrasonic atomizer may work but requires development.

403 *Combustion kinetics*: The model above is based primarily on thermodynamics, and studies
404 referenced above have shown hydride particle breakup can accelerate combustion. But designing an engine
405 will require more quantitative measurement of combustion kinetics. How quickly do the particles combust,
406 and is there any breakup associated with $MgH_2$ decomposition? How rapidly does Mg evaporate in the
407 flame? Will $NO_x$ formation be influenced due to the different flame structure compared to HC combustion?
408 What will the burning rates be at engine-relevant conditions *i.e.* how does the burning rate change with
409 pressure? Will the exhaust MgO particle agglomeration rates grow with pressure?
410 *Turbine blade erosion or deposition*: The effects of MgO particles on turbine blades, including
411 their thermal barrier coatings, are unknown. Particle size should be similar to that of soot, and particles
412 should mostly follow streamlines. But the number of MgO particles will be orders of magnitude higher
413 than soot.
414 *Aircraft design*: The Breguet range equation calculation above showed that for an existing aircraft
415 design, substituting slurry for jet fuel should achieve longer range. But it is likely possible to change the
416 design to optimize lift/drag for the higher density of this fuel, and structural enhancements will also be
417 necessary. These may slightly reduce or perhaps enhance the range advantage of this fuel.
418 *Weather and climate impacts*: If MgO nanoparticles attract liquid water, they may modify
419 precipitation patterns and the atmospheric water balance. Their high refractive index of 1.73 could reflect
420 solar radiation (higher than $CaCO_3$ at 1.59 suggested by others [39]); droplet formation and effects on
421 atmospheric water vapor could also alter infrared absorption. On the other hand, in addition to $CO_2$, more
422 alkaline aerosols could absorb and precipitate out $SO_2$, NOx, and halides, which could improve climate
423 forcing and ozone stability [39], and maybe even react with and reduce the atmospheric residence times of
424 chlorofluorocarbons, perfluorocarbons and hydrofluorocarbons [40, 41].
425 *Biosphere impacts*: Although high $Mg^{2+}$ concentration in the oceans will make changes to marine
426 life negligible, alkaline precipitation will have unknown effects on land watersheds.
427 *Localized impacts around airports*: Though dilute $MgCO_3$-$Mg(HCO_3)_2$ rain will likely have
428 negligible impacts on human health, concentrations near airports would be much higher and would likely

have significant impacts on health and the environment. MgO dust could collect on runways; mixed with rain this would create highly alkaline sludge. Burning hydrocarbon fuel during takeoff and switching to slurry fuel at cruising altitude would mitigate these effects at the cost of higher fuel system complexity. Emergency landings soon after takeoff would need to consider the different impacts of dumping slurry fuel *vs.* conventional fuel.

If this fuel concept becomes economical for aircraft, including emissions costs, it may also be advantageous for other fuel applications, such as ground transportation and stationary power generation. That said, the MgO particle atmospheric residence time for those applications is much lower, so particles would accumulate on the ground if not captured for other uses.

One way to think about $MgH_2$ in fuel is as an additive to promote direct air capture (DAC) and sequestration of $CO_2$. That is, it turns the traditional DAC plant inside out: instead of drawing large quantities of air through a bed of MgO, CaO or an aqueous slurry, this fuel disperses MgO into the atmosphere to do its job. Unlike DAC, this fuel has the additional benefit of propelling aircraft (with the limitations enumerated above), whereas the only benefit of DAC is cleaning the atmosphere. Completing the life cycle described above, when $MgH_2$ is produced from sea water or brines, the overall reaction is $MgCl_2(aq) + 2H_2O + CO_2(air) \rightarrow Mg(HCO_3)_2(aq) + 2\ HCl$, so if the HCl is kept out of the oceans, the lower acidity of $HCO_3^-$ than $Cl^-$ would *slightly* mitigate ocean acidification.

## 5. Concluding Remarks

Thermodynamic calculations presented here indicate that $MgH_2$-hydrocarbon slurry holds promise as a jet fuel substitute with lower, zero, or even negative net GHG emissions – without sacrificing aircraft range. In particular:

- The mass and volume ratios of slurry fuel to conventional fuel required to reach a given combustion temperature are slightly lower than would be expected based solely on the ratio of LHV specific energy or energy density.

- This effect is more pronounced at higher temperature, particularly above 2200 K, due to the greater stability of MgO vs. $CO_2$.
- The reduced moles of gas produced by $MgH_2$ combustion vs. hydrocarbons does not significantly mitigate this effect.
- Based on the higher LHV energy density of this fuel and the small added advantage of MgO stability, estimated aircraft range by the Breguet correlation is 8% longer than dodecane, 2.5 times longer than ammonia, and 3.5 times longer than liquid hydrogen for a given fuel tank volume, though this could be partially offset by additional structural requirements due to higher fuel density which were not considered in this study.
- Atmospheric equilibrium calculations and particle residence time scale estimates indicate that each mole of Mg in fuel burned at cruising altitude reacts with 1-2 moles of $CO_2$ in the atmosphere before reaching the earth's surface, which can dramatically reduce the GHG impact of air travel.
- That said, life cycle GHG impact depends strongly on the raw material and production method used to produce the $MgH_2$ slurry. In particular, magnesium metal production today has very high GHG emissions which would more than offset the benefits of this fuel, though there are processes in development and early deployment which could result in net negative GHG emissions.

Further feasibility assessment requires additional studies on atomization, combustion kinetics, engine and airframe design, and other environmental impacts, particularly in proximity to airports.

**Acknowledgements**

This work was supported by a TRIAD seed grant from Worcester Polytechnic Institute.

**References**


1. McCollum, D. L., Gould, G., & Greene, D. L. (2010). Greenhouse Gas Emissions from Aviation and Marine Transportation: Mitigation Potential and Policies. *California Digital Library, University of California Davis*.
2. Terrenoire, E., Hauglustaine, D. A., Gasser, T., & Penanhoat, O. (2019). The contribution of carbon dioxide emissions from the aviation sector to future climate change. Environmental Research Letters, 14(8), 084019. https://doi.org/10.1088/1748-9326/ab3086
3. Popp, J., Lakner, Z., Harangi-Rákos, M., & Fári, M. (2014). The effect of bioenergy expansion: Food, energy, and environment. Renewable and Sustainable Energy Reviews, 32, 559–578. https://doi.org/10.1016/j.rser.2014.01.056
4. Bergthorson, J. M. (2018). Recyclable metal fuels for clean and compact zero-carbon power. *Progress in Energy and Combustion Science*, 68, 169–196. doi: 10.1016/j.pecs.2018.05.001
5. Glassman, I., & Papas, P. (1999). Combustion Thermodynamics of Metal-Complex Oxidizer Mixtures. *Journal of Propulsion and Power,* 15(6), 801–805. doi: 10.2514/2.5499\
6. Daniel Krewski , Robert A Yokel , Evert Nieboer , David Borchelt , Joshua Cohen , Jean Harry , Sam Kacew , Joan Lindsay , Amal M Mahfouz & Virginie Rondeau (2007) Human Health Risk Assessment for Aluminium, Aluminium Oxide, and Aluminium Hydroxide, *Journal of Toxicology and Environmental Health*, Part B, 10:S1, 1-269, DOI: 10.1080/10937400701597766
7. Inan-Eroglu, E., & Ayaz, A. (2018). Is aluminum exposure a risk factor for neurological disorders? Journal of Research in Medical Sciences : *The Official Journal of Isfahan University of Medical Sciences*, 23. https://doi.org/10.4103/jrms.JRMS_921_17
8. Mcdonald, J. B., Dhakal, S., & Macreadie, I. (2021). A Toxic Synergy between Aluminium and Amyloid Beta in Yeast. *International Journal of Molecular Sciences*, 22(4), 1835. https://doi.org/10.3390/ijms22041835
9. R. F. Hamilton, S. A. Thakur, and A. Holian, "Silica binding and toxicity in alveolar macrophages," *Free Radical Biology and Medicine*, 44(7), 1246–1258, 2008. DOI: 10.1016/j.freeradbiomed.2007.12.027
10. Takeda, O., Ouchi, T. & Okabe, T.H. (2020). Recent Progress in Titanium Extraction and Recycling. *Metall Mater Trans* B 51, 1315–1328. https://doi.org/10.1007/s11663-020-01898-6
11. Volpe, S. L. (2013). Magnesium in Disease Prevention and Overall Health. *Advances in Nutrition*, 4(3). doi: 10.3945/an.112.003483
12. Kuschner, W. G., Wong, H., Dalessandro, A., Quinlan, P., & Blanc, P. D. (1997). Human Pulmonary Responses to Experimental Inhalation of High Concentration Fine and Ultrafine Magnesium Oxide Particles. *Environmental Health Perspectives*, 105(11), 1234. doi: 10.2307/3433903
13. P.R. Choudhury, Slurry fuels, Progress in Energy and Combustion Science 18 (1992), 409-427.
14. Gregory Young, Rohit Jacob & Michael R. Zachariah (2015) High Pressure Ignition and Combustion of Aluminum Hydride, *Combustion Science and Technology*, 187:9, 1335-1350, DOI: 10.1080/00102202.2015.1038383
15. Young, G., Piekiel, N., Chowdhury, S., & Zachariah, M. R. (2010). Ignition Behavior of α-AlH 3. *Combustion Science and Technology*, 182(9), 1341–1359. https://doi.org/10.1080/00102201003694834

16. J. Liu, J. Yuan, H. Li, A. Pang, P. Xu, G. Tang, X. Xu, Thermal oxidation and heterogeneous combustion of AlH3 and Al: A comparative study, Acta Astronautica (2020), doi: https://doi.org/10.1016/j.actaastro.2020.11.039.
17. Vigeholm, B., Kjoller, J., Larsen, B., & Pedersen, A. S. (1983). FORMATION AND DECOMPOSITION OF MAGNESIUM HYDRIDE. *Journal of the Less-Common Metals*, (89), 135–144.
18. Brown, K. S., Jr., Bowen, D. D. G., & McClaine, A. W. (2017). Methods and Systems for Making Metal Hydride Slurries (Australian Patent Office Patent No. 2014223195). https://patents.google.com/patent/AU2014223195B2/en
19. Andrew W. McClaine, Kenneth Brown and David D. G. Bowen, J. Energy Resour. Technol. 2015;137(6):061201-061201-9. doi:10.1115/1.4030398
20. Naik, C. V., Puduppakkam, K. V., Modak, A., Meeks, E., Wang, Y. L., Feng, Q., & Tsotsis, T. T. (2011). Detailed chemical kinetic mechanism for surrogates of alternative jet fuels. *Combustion and Flame*, 158(3), 434–445. doi: 10.1016/j.combustflame.2010.09.016
21. Vasu, S., Davidson, D., Hong, Z., Vasudevan, V., & Hanson, R. (2009). n-Dodecane oxidation at high-pressures: Measurements of ignition delay times and OH concentration time-histories. *Proceedings of the Combustion Institute*, 32(1), 173–180. doi: 10.1016/j.proci.2008.05.006
22. Law, C. K. (2006). *Combustion physics*. Cambridge University Press
23. David G. Goodwin, Raymond L. Speth, Harry K. Moffat, and Bryan W. Weber. Cantera: An object-oriented software toolkit for chemical kinetics, thermodynamics, and transport processes. https://www.cantera.org, 2021. Version 2.5.1. doi:10.5281/zenodo.4527812
24. Chase, M.W., Jr., NIST-JANAF Themochemical Tables, Fourth Edition, J. Phys. Chem. Ref. Data, Monograph 9, (1998), 1-1951.
25. A. Burcat. (2017), Thermochemical species in polynomial form. Technion - Israel Institute of Technology. https://burcat.technion.ac.il/.
26. Sirjean, B., Dames, E., Sheen, D. A., You, X.-Q., Sung, C., Holley, A. T., Egolfopoulos, F. N.,Wang, H.,Vasu, S. S., Davidson, D. F., Hanson, R. K., Pitsch, H., Bowman, C. T., Kelley, A., Law, C. K., Tsang, W., Cernansky, N. P., Miller, D. L., Violi, A., and Lindstedt, R. P., "A High-Temperature Chemical Kinetic Model of n-Alkane Oxidation, JetSurF Version 1.0," http://melchior.usc.edu/JetSurF/JetSurF1.0/index.html [retrieved 15 Sept. 2009].
27. Turns, S. R. (2012). *An Introduction to Combustion: Concepts and Applications, 3rd edition*. McGraw Hill
28. "Trent 1000 infographic"(2016). Rolls-Royce. https://www.rolls-royce.com/site-services/images/trent-1000-infographic.aspx
29. J.E.A. John, T.G. Keith, (2006). Gas Dynamics, Pearson, New York, New York
30. Lomba, R., Bernard, S., Gillard, P., Mounaïm-Rousselle, C., Halter, F., Chauveau, C., Tahtouh, T., & Guézet, O. (2016). Comparison of Combustion Characteristics of Magnesium and Aluminum Powders. *Combustion Science and Technology*, 188(11–12), 1857–1877. https://doi.org/10.1080/00102202.2016.1211871
31. Chunmiao, Y., Lifu, Y., Chang, L., Gang, L., & Shengjun, Z. (2013). Thermal analysis of magnesium reactions with nitrogen/oxygen gas mixtures. *Journal of Hazardous Materials*, 260, 707–714. doi: 10.1016/j.jhazmat.2013.06.047
32. C. Anastasio and S. T. Martin, "Atmospheric Nanoparticles," *Reviews in Mineralogy and Geochemistry*, 44(1), 293–349, Jan. 2001, doi: 10.2138/rmg.2001.44.08.

33. Schmidt, O., Melchior, S., Hawkes, A., & Staffell, I. (2019). Projecting the Future Levelized Cost of Electricity Storage Technologies. *Joule*, 3(1), 81–100. https://doi.org/10.1016/j.joule.2018.12.008
34. Ehrenberger, S. (2020). Carbon Footprint of Magnesium Production and its Use in Transport Applications. International Magnesium Association. https://cdn.ymaws.com/www.intlmag.org/resource/resmgr/sustainability/2020-LCA-Study-2021-02-09.pdf
35. Rutherford, M., Telgerafchi, A. E., Espinosa, G., Powell, A. C., & Dussault, D. (2021). Low-Cost Magnesium Primary Production Using Gravity-Driven Multiple Effect Thermal System (G-METS) Distillation. *Magnesium 2021*, 139–144. https://doi.org/10.1007/978-3-030-65528-0_21
36. Cherubini, F., Raugei, M., & Ulgiati, S. (2008). LCA of magnesium production. Resources, Conservation and Recycling, 52(8–9), 1093–1100. https://doi.org/10.1016/j.resconrec.2008.05.001
37. Ehrenberger, S., & Friedrich, H. E. (2013). Life-Cycle Assessment of the Recycling of Magnesium Vehicle Components. *JOM*, 65(10), 1303–1309. https://doi.org/10.1007/s11837-013-0703-3
38. Gibbs, J. B., & Cook, P. N. (1952). PREPARATION AND PHYSICAL PROPERTIES OF METAL SLURRY FUELS (NACA RM E52A23; p. 38). *National Advisory Committee for Aeronautics*.
39. Keith, D. W., Weisenstein, D. K., Dykema, J. A., & Keutsch, F. N. (2016). Stratospheric solar geoengineering without ozone loss. *Proceedings of the National Academy of Sciences*, 113(52), 14910–14914. https://doi.org/10.1073/pnas.1615572113
40. Lee, M. C., & Choi, W. (2004). Development of thermochemical destruction method of perfluorocarbons (PFCs). *Journal of Industrial and Engineering Chemistry*, 10(1), 107–114.
41. Kato, S., Takeuchi, A., & Watanabe, T. (2001). Integrated Process for Disposal of Halon 1301 (CBrF3) with Calcined Dolomites and Limestones. 8.